

AD-A156 694

POTENTIAL STRUCTURES AND PARTICLE ACCELERATION ON
AURORAL FIELD LINES(U) AEROSPACE CORP EL SEGUNDO CA
SPACE SCIENCES LAB D J GORNEY 01 MAY 85
TR-0084A(5940-05)-6 SD-TR-85-12

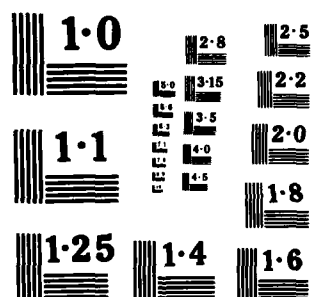
1/1

UNCLASSIFIED

F/G 4/1

NL

END
8 85



AD-A156 694

DTIC FILE

Prepared for
SPACE DIVISION
AIR FORCE SYSTEMS COMMAND
Los Angeles Air Force Station
P.O. Box 92960, Worldway Postal Center
Los Angeles, CA 90009-2960

85 7 08 102


This report was submitted by The Aerospace Corporation, El Segundo, CA 90245, under Contract No. F04701-83-C-0084 with the Space Division, P.O. Box 92960, Worldway Postal Center, Los Angeles, CA 90009. It was reviewed and approved for The Aerospace Corporation by H. R. Rugge, Director, Space Sciences Laboratory. Lt Douglas R. Case, SD/YCC, was the project officer for the Mission Oriented Investigation and Experimentation Program.

This report has been reviewed by the Public Affairs Office (PAS) and is releasable to the National Technical Information Service (NTIS). At NTIS, it will be available to the general public, including foreign nationals.

This technical report has been reviewed and is approved for publication. Publication of this report does not constitute Air Force approval of the report's findings or conclusions. It is published only for the exchange and stimulation of ideas.



Douglas R. Case, 1st Lt, USAF
Project Officer



Joseph Hess, GM-15, Director, West Coast
Office, AF Space Technology Center

UNCLASSIFIED

SECURITY CLASSIFICATION OF THIS PAGE (When Data Entered)

REPORT DOCUMENTATION PAGE		READ INSTRUCTIONS BEFORE COMPLETING FORM
1. REPORT NUMBER SD-TR-85-12	2. GOVT ACCESSION NO. AD A156 694	3. RECIPIENT'S CATALOG NUMBER
4. TITLE (and Subtitle) POTENTIAL STRUCTURES AND PARTICLE ACCELERATION ON AURORAL FIELD LINES		5. TYPE OF REPORT & PERIOD COVERED
7. AUTHOR(s) David J. Gorney		6. PERFORMING ORG. REPORT NUMBER TR-0084A(5940-05)-6
9. PERFORMING ORGANIZATION NAME AND ADDRESS The Aerospace Corporation El Segundo, Calif. 90245		8. CONTRACT OR GRANT NUMBER(s) EO4701-83-C-0084
11. CONTROLLING OFFICE NAME AND ADDRESS Space Division Los Angeles Air Force Station Los Angeles, Calif. 90009		10. PROGRAM ELEMENT, PROJECT, TASK AREA & WORK UNIT NUMBERS
14. MONITORING AGENCY NAME & ADDRESS (if different from Controlling Office)		12. REPORT DATE 1 May 1985
		13. NUMBER OF PAGES 29
		15. SECURITY CLASS. (of this report) Unclassified
16. DISTRIBUTION STATEMENT (of this Report) Approved for public release; distribution unlimited.		15a. DECLASSIFICATION/DOWNGRADING SCHEDULE
17. DISTRIBUTION STATEMENT (of the abstract entered in Block 20, if different from Report)		
18. SUPPLEMENTARY NOTES		
19. KEY WORDS (Continue on reverse side if necessary and identify by block number) Aurora, Electric Fields		
20. ABSTRACT (Continue on reverse side if necessary and identify by block number) In the 1970's major advances in the understanding of auroral processes were brought about by observations of plasmas and electric fields within the regions of space responsible for auroral particle acceleration. The major contribution of these observations was the verification of the existence of electric fields with components parallel to the magnetic field over large regions of altitude (1000-20000 kilometers). These electric fields constitute potential drops of several kilovolts, accelerating magnetospheric		

DD FORM 1473
(FACSIMILE)

UNCLASSIFIED

SECURITY CLASSIFICATION OF THIS PAGE (When Data Entered)

UNCLASSIFIED

SECURITY CLASSIFICATION OF THIS PAGE(When Data Entered)

19. KEY WORDS (Continued)

about

20. ABSTRACT (Continued)

electrons downward to form the aurora and ionospheric ions upward, where they contribute significantly to the magnetospheric hot ion population. Perpendicular spatial scales of ~ 100 kilometers are most common, although finer scales have been observed embedded, and individual small amplitude double layers occur on much smaller parallel spatial scales.

More recently, these same data sets have revealed the existence of ~ 100 V electric potential drops directed downward in return current regions. Downward electric fields are in a direction to accelerate electrons out of the ionosphere and tend to retard the propagation of ions upward. An association between upflowing electron beams and transversely heated ions at low altitude has been noted, and a causal relationship between downward electric fields and ion conics is suggested.

UNCLASSIFIED

SECURITY CLASSIFICATION OF THIS PAGE(When Data Entered)

CONTENTS

INTRODUCTION.....	5
OBSERVATIONS - INVERTED-V REGION.....	9
OBSERVATIONS - RETURN CURRENT REGION.....	19
SUMMARY.....	29
REFERENCES.....	31



DTIC	
COPY	
INSPECTED	
1	
Distribution/	
Availability Codes	
Avail and/or	
Dist	Special
A-2	

FIGURES

1. A Diagram Depicting the Particle Populations and Inferred Electric Field Structures Which are Common to the Low Altitude Auroral Flux Tube and Return Current Region..... 6
2. A Composite Plot of an S3-3 Energy-Time Particle Spectrogram and the Measured Perpendicular Electric Field for an Auroral Crossing in the Dusk Sector Near $1 R_E$ Altitude..... 10
3. A Plot of the Perpendicular Electric Field Components Observed on S3-3 from 41040-41340 seconds U.T. on 29 July 1976..... 11
4. An Example of S3-3 Electric Field Observations Including the Electric Field Component Parallel to the Local Magnetic Field, Showing the Existence of Small-Amplitude Double Layers in Space..... 13
5. A Plot Describing the Expected Organization of Magnetospheric (M), Ionospheric (I) and Secondary (S) Electron Populations in the Presence of a Potential Drop V 15
6. Plots of the Electron and Ion Distribution Function in Parallel and Perpendicular Velocity..... 16
7. Examples of Transversely Heated Ion Distributions (Ion Conics) Observed by the S3-3 Satellite Within and Above the Heating Altitude..... 20
8. Data from the ISIS-2 Spacecraft Showing the Occurrence of Upflowing Field-Aligned Electron Beams in Association with Ion Conics..... 22
9. A Plot of Computed Ion Trajectories in v and Altitude (h) with a Heating Rate of 1 eV/sec and Parallel Electric Field of $E_{\parallel} = -0.1$ mV/m Over the Altitude Range $0.1 R_E < h < 1.0 R_E$ 25
10. A Plot Showing the Computed Ion Pitch Angle Distributions at Altitudes 1000, 5000, 6000, and 7000 km..... 27

INTRODUCTION

One of the major advances in space research during the past decade has been the verification of the existence of electric fields in the earth's auroral regions with components parallel to the geomagnetic field /1,2/ over a large altitude range.

More recently, evidence for parallel electric fields adjacent to the auroral region has also emerged /3,4,5/, leading to a view of the low-altitude auroral region as depicted in Figure 1. This schematic diagram shows two regions of high-latitude particle acceleration due to electric fields: the auroral flux tube in which an upward field aligned current is carried by magnetospheric electrons which are accelerated downward, and a return current region in which ionospheric electrons are accelerated upward.

In Figure 1, geomagnetic field lines are depicted by thin lines while electrical equipotential contours are drawn with thick lines. The diagram is meant to represent a region corresponding to an ionospheric horizontal scale of about 100 kilometers and a vertical scale of several thousand kilometers. The irregular distribution of electrical equipotentials within the auroral flux tube indicates the possible presence of both parallel and perpendicular structure on smaller scales. The equipotential contours are shown to return to high altitude, producing a V-shaped electric potential structure with no significant perpendicular electric field at ionospheric altitudes. A field-aligned potential drop could be accomplished equally well with an S-shaped electric potential structure. An S-shaped electric potential structure is drawn adjacent to the inverted-V region in Figure 1, depicting a downward-directed electric field in the return current region. Indeed, both S-shaped and V-shaped electric potential structures have been inferred from satellite data /6,7/.

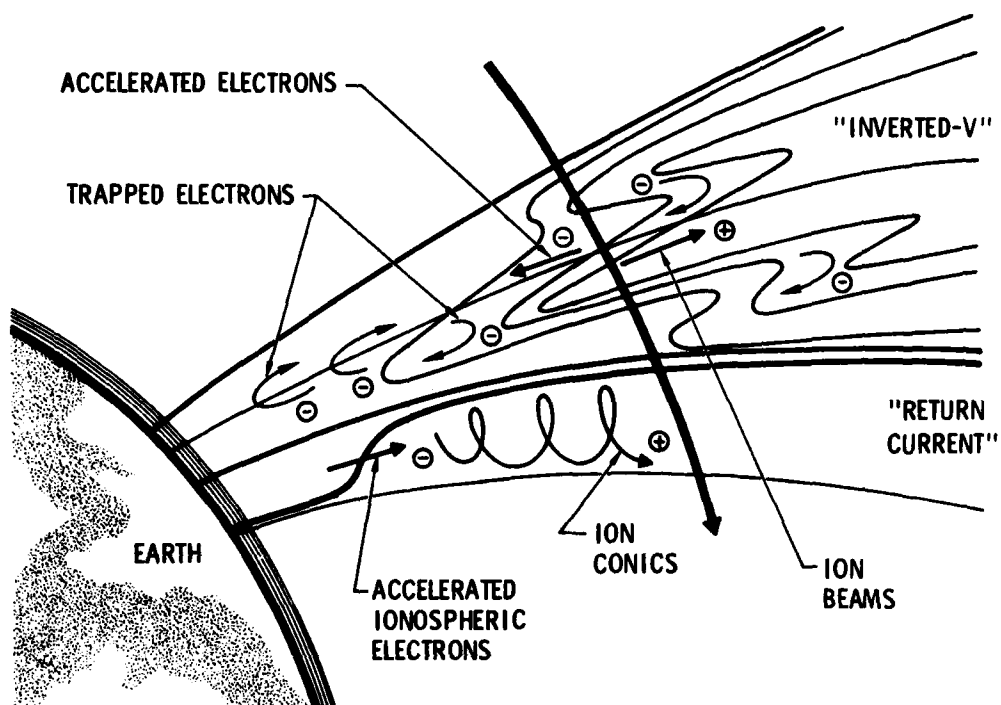


Figure 1. A diagram depicting the particle populations and inferred electric field structures which are common to the low altitude auroral flux tube and return current region.

7

A number of particle populations which are expected to arise within the inverted-V potential structure and adjacent return current regions are also indicated in Figure 1. Within the inverted-V one finds downward accelerated 1-10 keV electrons of magnetospheric origin and upflowing field-aligned ion beams of ionospheric origin. At low energies, electrons can become trapped at low altitudes between a magnetic mirror point above the atmosphere and an electrostatic mirror point at high altitudes. This trapped electron population is expected to have a counterstreaming velocity distribution at energies below that of the downflowing electron beam. In the return current region a reversed parallel electric field /8/ is expected to cause upward acceleration of ionospheric electrons to energies of perhaps tens or hundreds of electron volts. Current-driven instabilities arising from these upflowing electron beams at low altitudes are expected to cause turbulent transverse heating of local ionospheric ions /9,10/ which can be observed at all altitudes.

The intent of this report is to review particle and field observations acquired within and adjacent to the regions of space responsible for auroral particle acceleration. The observations are described, wherever possible, within the context of the electric field spatial structures depicted in Figure 1. Also, an effort is made in this review to demonstrate the important implications of downward-directed electric fields in the return current regions to the problem of transverse heating of ions.

1

OBSERVATIONS - INVERTED-V REGION

Examples of particle and field data acquired by the low-altitude S3-3 satellite while it passed through a number of regions of particle acceleration are shown in Figure 2. The figure shows electron (.17-30 keV) and ion (.09-3.9 keV) energy flux versus time along with a plot of one of the electric field components perpendicular to the geomagnetic field. Note that the ion energy scale is reversed and the particle data is modulated (in pitch angle) at the satellite spin period of 20 seconds.

During the 20-minute segment of data shown in Figure 2 S3-3 crosses a number of particle acceleration events most notably those at 41090, 41160 and 41250 seconds U.T. and a broad acceleration region from 41280-41440 seconds U.T. Within these acceleration regions the energy of precipitating electrons increases (i.e., the standard inverted-V signature /11/) and upflowing field-aligned ion beams are observed. The correlation in space and time between upward ion and downward electron acceleration is strong evidence for acceleration by parallel electric fields which extend over a broad range of altitude. Acceleration of ions transverse to the magnetic field is evident in regions between the inverted-V signatures, most notably near 40850-41000 seconds U.T. and near 41200 seconds U.T. These heated ions have fluxes which peak twice per satellite spin, and have been called ion conics because of the ions' conical distribution in velocity space.

Each of the regions of parallel electron and ion acceleration are associated with strong signatures in the perpendicular electric field. These electrostatic shocks /2/ have amplitudes in excess of 400 mV/m. The perpendicular electric field observations from 41040-41340 seconds U.T. are shown in an expanded plot in Figure 3.

Concentrating on the x-component of the electric field, corresponding roughly to the equatorward component, one sees that as S3-3 flies from low toward high latitude it observes perpendicular electric fields which are first poleward then equatorward through the regions of particle acceleration. These perpendicular electric field signatures occur over local spatial scales

S3-3, 29 JULY 1976

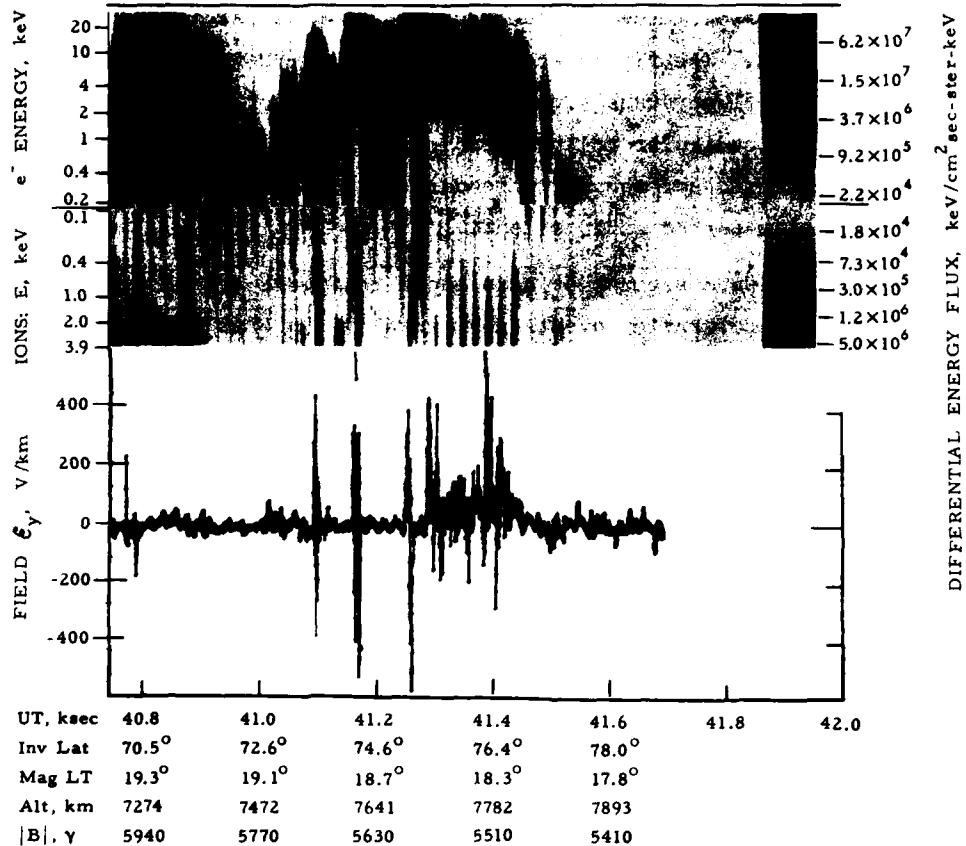


Figure 2. A composite plot of an S3-3 energy-time particle spectrogram and the measured perpendicular electric field for an auroral crossing in the dusk sector near $1 R_e$ altitude.

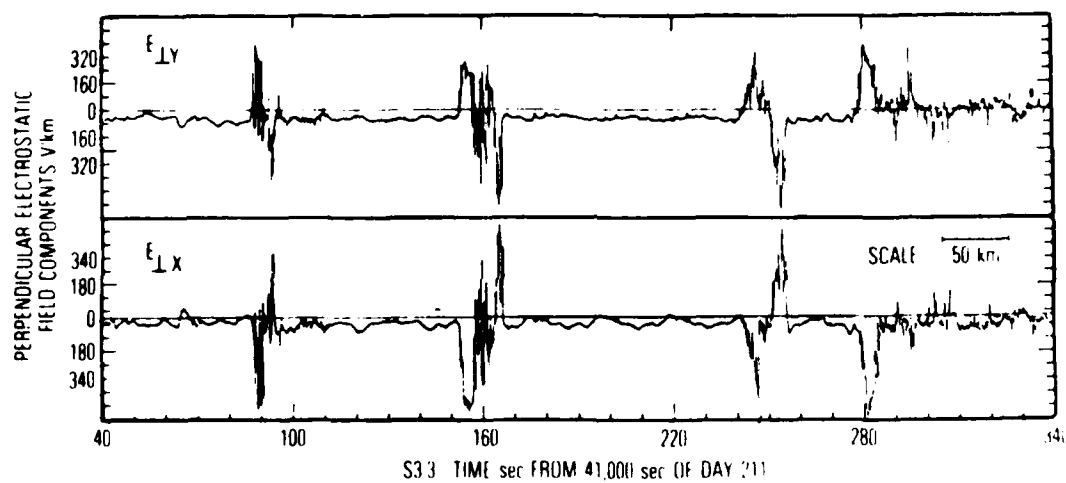


Figure 3. A plot of the perpendicular electric field components observed on S3-3 from 41040-41340 seconds U.T. on 29 July 1976.

of 50 kilometers and are of a polarity which is consistent with that sketched in Figure 1. It has been shown that the potential drop across these shocks scales directly with the upflowing ion beam energy within the shock /12/, implying a causal association between the V-shaped electric field structures and ion beams.

Direct observations of the parallel component of the electric field have proved to be extremely difficult to accomplish, but recently signatures of small-amplitude double layers have been recognized in the electric field data of the S3-3 satellite /13,14/. An example of a direct observation of double layers from the electric field instrument on S3-3 is shown in Figure 4. Three electric field components are plotted in Figure 4, with an amplitude scale in the upper left. The figure shows approximately 0.4 seconds of data.

The dominant signature in the perpendicular electric field in Figure 4 is the appearance of a 100 Hz oscillation, most apparent in the upper plot. This is the signature of electrostatic hydrogen cyclotron waves, which are known to be associated with acceleration regions and ion beams /15/. Clearly visible in the plot of the parallel electric field component are about ten single-polarity spikes, with amplitudes of 1-10 mV/m. The total potential drop across these double layers has been estimated at about a volt, and they appear to be passing the spacecraft at approximately 50 km/s /13/. If the total auroral potential drop of a few kilovolts is due to the summed effect of these small-amplitude double layers, one would require thousands of double layers distributed over several thousand kilometers, since the average parallel electric field due to double layers would be $\lesssim 1$ mV/m. Due to the difficulties involved in observing double layers, no substantial survey of their occurrence frequencies or distribution has been accomplished.

Turning to the energetic particle observations within these electric field structures, we might first refer to Figure 5 which describes the expected organization of electrons in the presence of upward parallel electric field /16/.

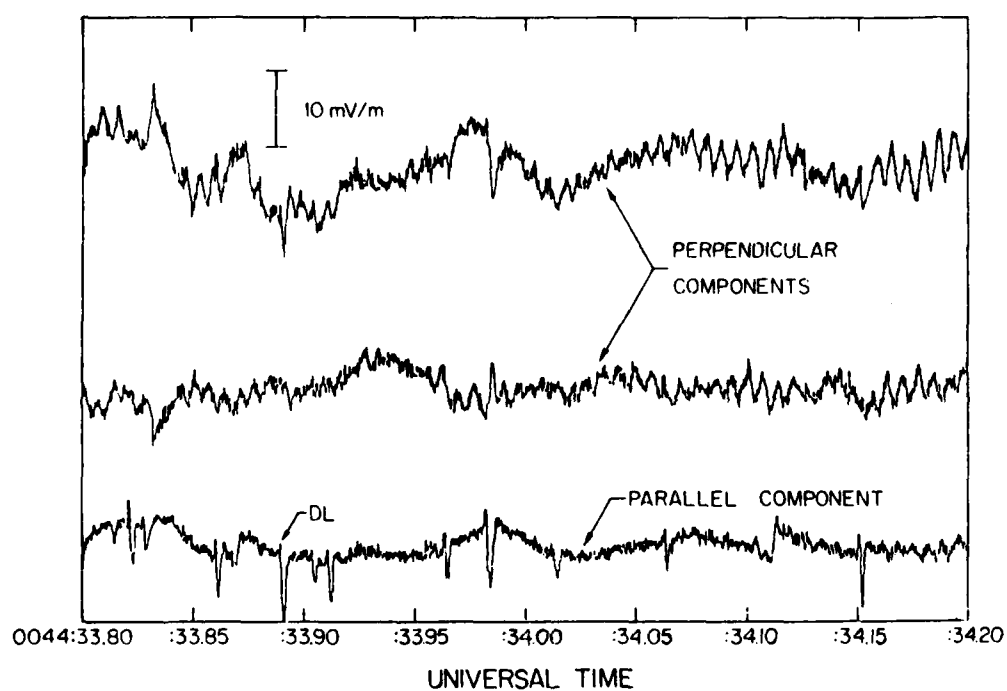


Figure 4. An example of S3-3 electric field observations including the electric field component parallel to the local magnetic field, showing the existence of small-amplitude double layers in space.

Under the influence of a potential drop between the distant magnetosphere and the point of observation, the accelerated magnetospheric electron population should be found external to an elliptical boundary whose axes depend on the strength of the potential and whose eccentricity depends on the magnetic field ratio of the system. In the earth's magnetospheric system the magnetic field ratio is quite large (~ 10 - 100) and one would expect this elliptical boundary to degenerate to a circle for particle observations at low altitudes. Nominal atmospheric loss-cone boundaries become modified due to a potential difference between the atmosphere and the point of observation to form the hyperbolic loss-cone boundary shown in the figure. Note that the greatest modification exists at the lowest particle velocities, and the modification is such that the loss cone becomes exaggerated at low energies. A region of velocity space can form, labeled T in Figure 5, corresponding to particles which mirror above the atmosphere but are trapped below the electrical potential barrier at high altitudes. This representation of the organization of electron populations in velocity space has proved quite useful in interpreting particle observations within inverted-Vs. Actual particle observations within an inverted-V are shown in the form of contour plots of particle distribution functions for electrons (left) and ions (right) in Figure 6.

The accelerated magnetospheric electron population in Figure 6 is the isotropic (in pitch angle) population exceeding a velocity of 0.3×10^5 km/sec. Again, a field-aligned electron beam is not expected, due to the high magnetic field ratio in the magnetospheric system. A strong signature of the atmospheric loss cone is apparent in the electron distribution, particularly at low velocities where the loss-cone angle is exaggerated. A mirror image of the loss-cone is observed in the downflowing direction at low velocities due to the reflection of low energy particles by the electrical potential barrier at high altitude. The trapped electron population is quite distinct in this example, since it has a velocity distribution quite different from that of the accelerated or loss-cone populations. The trapped electrons are distributed uniformly in parallel velocity, perhaps due to the long-term summed effect of wave particle interactions.

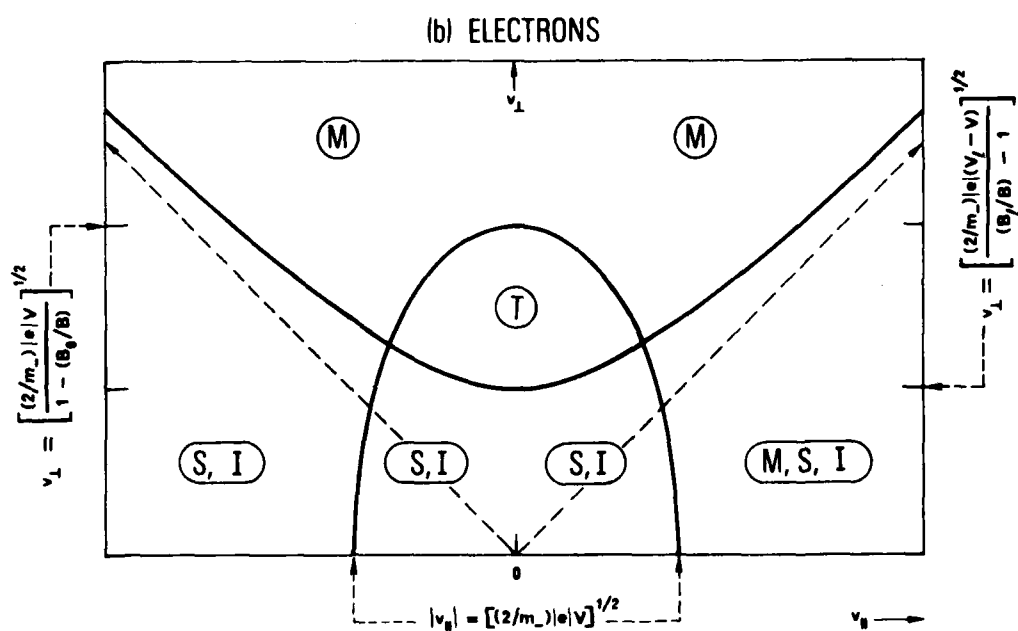


Figure 5. A plot describing the expected organization of magnetospheric (M), ionospheric (I) and secondary (S) electron populations in the presence of a potential drop V . Positive v_{\parallel} refers to downstreaming particles.

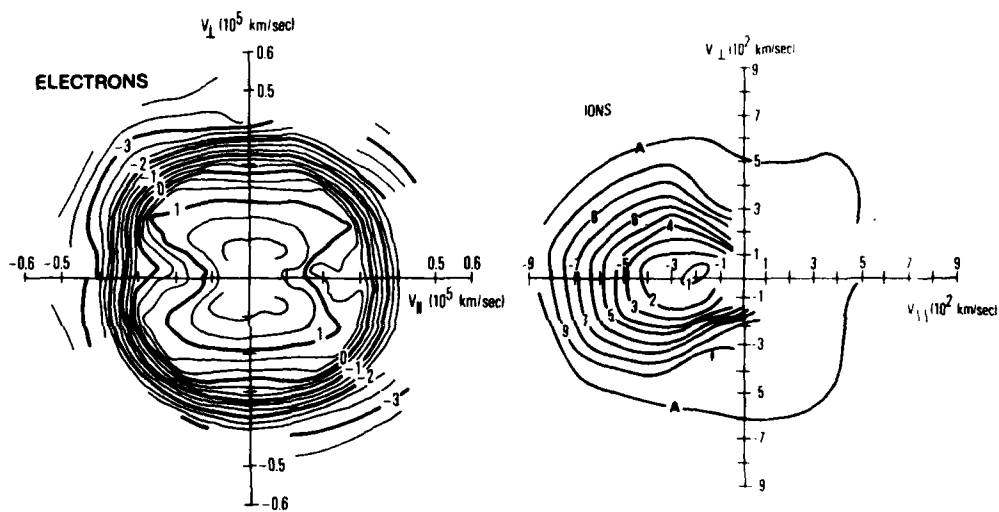


Figure 6. Plots of the electron and ion distribution function in parallel and perpendicular velocity. Contours are logarithmic, with labels corresponding to exponents of the power ten in units of sec^3/km^6 .

7

The ion distribution in this case is a classic example of an upflowing field-aligned ion beam. The obvious interpretation of the ion beam is that ionospheric ions have been accelerated upward along the auroral field lines to keV energies. Statistical studies have shown that a significant fraction of this ion acceleration occurs in the $1 R_e$ altitude region /17,18/. These ionospheric ions must undergo substantial parallel and perpendicular heating in order to account for the observed ion beam temperatures. This heating is not surprising since large-amplitude ion cyclotron waves occur commonly in inverted-V's /15/.

It should be noted that the particle observations shown here were acquired well within inverted-V's, and they certainly contain a number of signatures attributable to acceleration by parallel electric fields. Particle observations near the edges of inverted-V's show more complicated velocity distributions /19/, indicating that other mechanisms might act along with parallel electric fields to redistribute particles in velocity space.

OBSERVATIONS - RETURN CURRENT REGION

Within the return current region, field aligned currents are expected to be carried primarily by cold ionospheric electrons flowing upward. This downward current region is expected to be unstable to electrostatic hydrogen and oxygen cyclotron waves. The ions are expected to be heated preferentially in perpendicular temperature, producing a pronounced "pancake" distribution in velocity space. Indeed, highly anisotropic heated ion distributions have been observed within and above the heating region, and two characteristic examples are shown in Figure 7. The ion conic example on the left of Figure 7 shows a heated ion distribution within the heating region, and the ions have a very anisotropic "pancake" distribution extending to keV energies. In the example on the right, the peak ion flux is at an intermediate angle between mirroring (90°) and upflowing (180°) directions, producing a conical distribution in velocity space. The general interpretation is that observations such as the right panel of Figure 7 are acquired above the heating region, where the ions show the focussing effect of the magnetic mirror force. By mapping ion conics to their mirror (source) point it has been determined that the dominant heating region is near 2000 km altitude /18/.

A great deal of experimental and theoretical work has been performed in order to determine the mechanism responsible for the very efficient heating which causes ion conics. A number of important observations associating the occurrence of ion conics with field-aligned currents have been noted. In particular, data from the ISIS-2 spacecraft have been used to demonstrate an apparent threshold effect in the dependence of ion heating on parallel current density /3/. An association between ion conics and field-aligned current density is not surprising since it is known that observed low-frequency wave amplitudes also scale with field-aligned current strength /20/. A problem exists, however, in that attempts to identify the plasma wave mode responsible for ion heating have proved somewhat disappointing. Observed wave amplitudes (e.g., hydrogen cyclotron waves, lower hybrid waves) in the region of heating are substantially lower /21/ than that required for the inferred particle

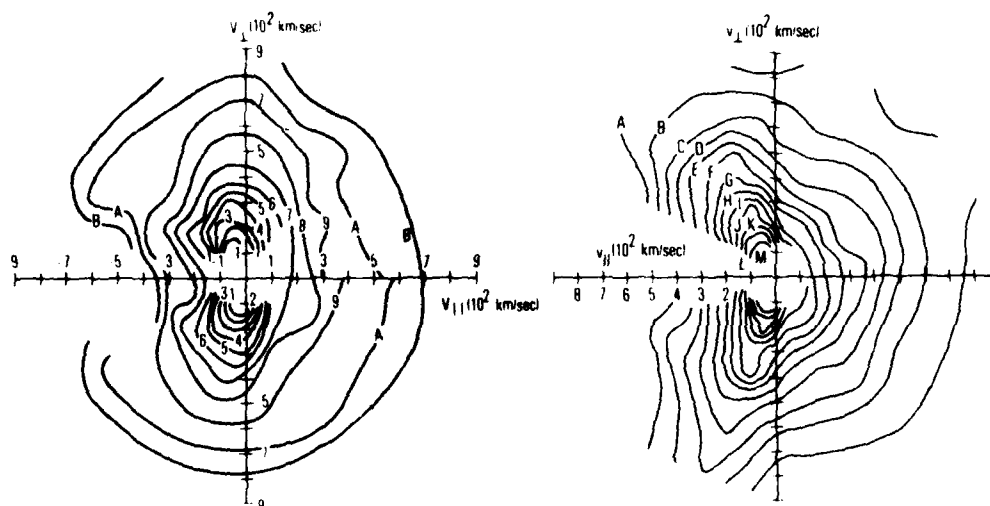


Figure 7. Examples of transversely heated ion distributions (ion conics) observed by the S3-3 satellite within (left) and above (right) the heating altitude.

heating rates. The fundamental problem with producing energetic ion conics is that heating rates must be very large in order to produce the observed mirror point ion energies before the magnetic mirror force expels the ions from the heating region. Fortunately recent satellite observations and theoretical descriptions of the return current regions have unveiled new insights into the ion conic generation mechanism. Theoretical models have predicted the existence of downward-directed potential drops along return current field lines /8/. If present, these downward electrical potential drops might retard the propagation of ions out of the heating region, leading to enhanced net heating /5/. Observational evidence for the existence of downward potentials has begun to emerge /3,4,5/ and an example is shown in Figure 8.

Figure 8 presents ion and electron data from the ISIS-2 spacecraft as a function of time, over a period in which the instrument scanned a complete range of pitch angles (center panel). The data clearly show the occurrence of intense upflowing field-aligned electron beams (indicated by upward arrows) in association with transversely accelerated ions (note peaks in ion flux at 90° pitch angles). These electron data have been interpreted as signatures of downward potentials of a few tens of volts between the atmosphere and the point of observation. Upward acceleration of ionospheric electrons to hundreds of electron volts has been observed at higher altitudes /5/.

A downward parallel electric field in the return current region would significantly modify the accepted picture of ion conic formation. Downward parallel electric potential drops of sufficient magnitude could balance or overcome the magnetic mirror force on the ions, trapping them at low altitude and preventing propagation upward until the ion kinetic energy becomes greatly enhanced through multiple-pass wave-particle heating. For trapping, the downward force due to the electric field must at least balance the magnetic mirror force. That is,

$$qE_{\parallel} = \mu \frac{dB}{dz} = \epsilon_1 \frac{d \ln B}{dz} \quad (1)$$

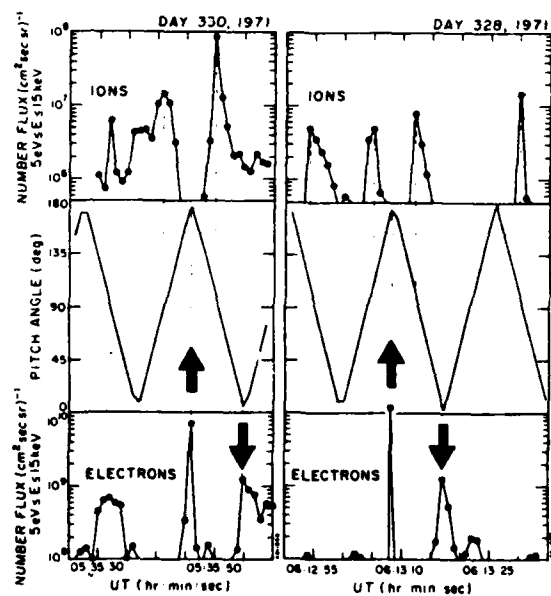


Figure 8. Data from the ISIS-2 spacecraft showing the occurrence of upflowing field-aligned electron beams in association with ion conics. The figure shows two examples of the phenomenon, in which electrons of ionospheric origin have been accelerated upward to energies of a few tens of electron volts.

where q is the charge, μ the magnetic moment, ϵ_{\perp} is the perpendicular energy and z is the distance along the magnetic field line. The critical parallel electric field for trapping is approximately

$$E_{\parallel} \text{ (mV/m)} = 0.471 \frac{\epsilon_{\perp} \text{ (keV)}}{z \text{ (R}_e\text{)}} \quad (2)$$

As an example, for $\epsilon_{\perp} = 100$ eV at 2000 km altitude (typical ion conic parameters) we get $E_{\parallel} \approx 0.04$ mV/m. For a distributed electric field this corresponds to a potential drop of 40 volts per 1000 kilometers. Note that the parallel electric field required to trap a 100 eV perpendicular ion conic at low altitude is quite reasonable compared with that inferred from S3-3, ISIS-2, and DE-1 observations. Ion trapping, enhanced heating, and escape might be a general sequence of events leading to ion conics.

The trajectories of ions in a region of downward parallel electric field and heating could be quite complicated and strongly dependent on the distribution of electric fields and heating in altitude. However, some important characteristics of ion trajectories in a trapping environment can be demonstrated using a straightforward test-particle approach /22/.

Although test-particle calculations cannot reproduce effects due to the collective behavior of the plasma (e.g., diffusion), valuable information can be gained on the access of particles to regions of space and velocity space.

One can rather simply describe the trajectory of an ion in velocity (v_{\parallel} , v_{\perp}) and distance along a magnetic field line (z) including the effects of a parallel electric field (E_{\parallel}), perpendicular energy gain due to wave-particle interactions $(d\epsilon_{\perp}/dt)_{WPI}$, and parallel/perpendicular momentum transfer due to propagation along a converging magnetic field. Thus, the parallel momentum equation can be written

$$m \frac{dv_{\parallel}}{dt} = eE_{\parallel} - \epsilon_{\perp} \frac{d \ln B}{dz} \quad (3)$$

where all the symbols have their standard meanings. The perpendicular energy of the particle is determined by propagation of the particle along the converging magnetic field, but is modified by wave-particle perpendicular acceleration. Thus,

$$\frac{d\epsilon_{\perp}}{dt} = v_{\parallel} \epsilon_{\perp} \frac{d \ln B}{dz} + \left(\frac{d\epsilon_{\perp}}{dt} \right)_{WPI} \quad (4)$$

This system of equations can be solved iteratively for the trajectory in velocity (v_{\parallel} , v_{\perp}) and altitude ($h = z - 1$). We use a simple model including a uniform parallel electric field $E = -0.1$ mV/m and a uniform perpendicular heating rate $(d\epsilon_{\perp}/dt)_{WPI} = 1$ eV/sec over the altitude range $0.1 R_e < h < |R_e$. Figure 9 shows the evolution of an ion trajectory in perpendicular velocity and altitude. The ion is released at zero velocity at an altitude of $0.1 R_e$, and the resulting trajectory (1) is plotted at one second time intervals. Initially the particle is energized by the simulated wave-particle interaction. Once it acquires significant perpendicular energy the particle is forced upward due to the magnetic mirror force. The particle propagates upward, exchanging perpendicular for parallel momentum, but losing kinetic energy because of the downward parallel electric field. Eventually the particle is reflected and executes a number of trapped bounces while gaining more perpendicular energy through wave-particle acceleration. Note that in executing the trapped portion of the trajectory the highest particle energy occurs at the low-altitude mirror point. In the case shown the particle escapes at a pitch angle of 135° and an energy just under 200 eV, whereas it attains an energy well above 600 eV within the trapping region. For reference, a second trajectory (2) is plotted which describes the ion motion in the absence of a parallel electric field. In this case [with the same heating rate as case (1)] the ion would gain a maximum of just under 100 eV kinetic energy.

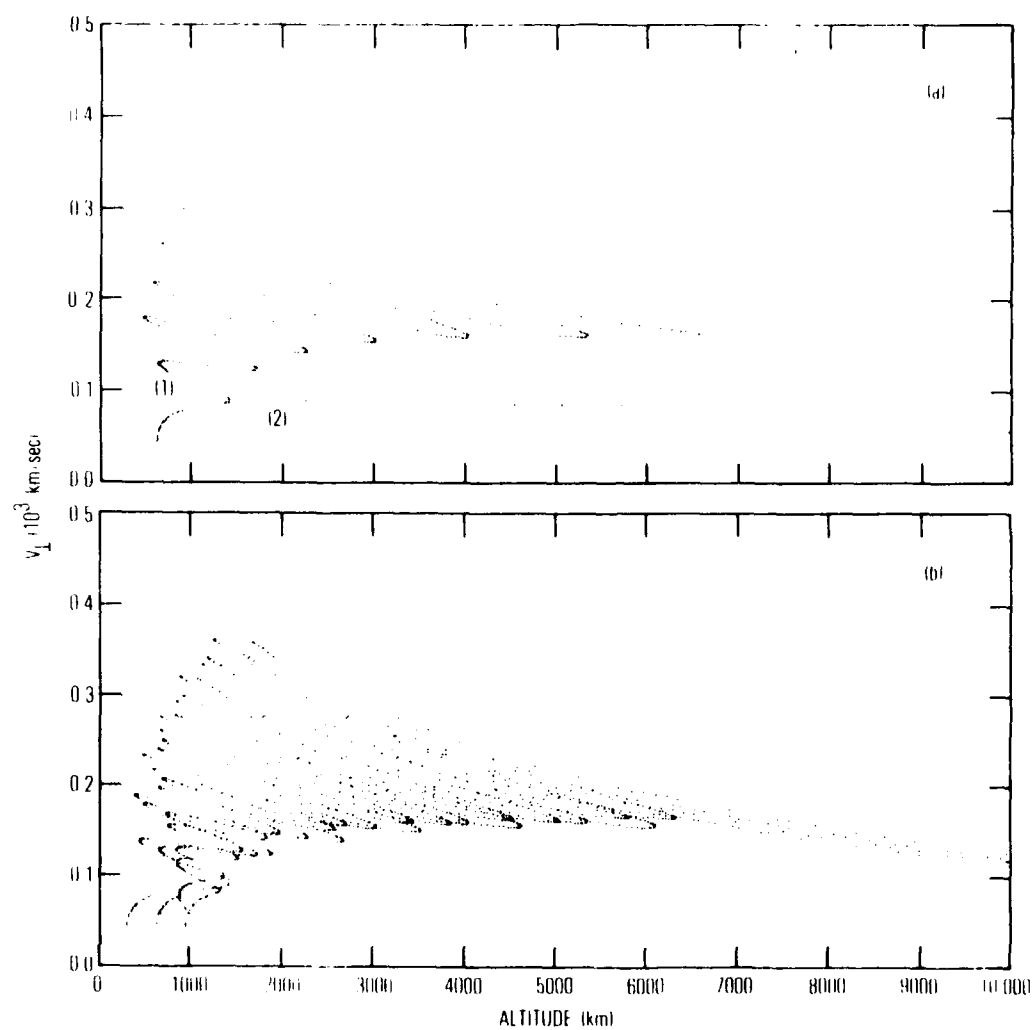


Figure 9. A plot of computed ion trajectories in v and altitude (h) with a heating rate of 1 eV/sec and parallel electric field of $E_{\parallel} = -0.1$ mV/m over the altitude range $0.1 R_e < h < 1.0 R_e$. The lower panel shows a composite of four trajectories.

The lower panel of Figure 10 shows a composite of several ion trajectories, starting over a range of altitude from $.05 R_e$ to $0.2 R_e$. It is apparent that the nature of the ion trajectories is not significantly affected by the starting point of the particle but is strongly governed by the imposed electric field model. Note that all particles have mirror points near $0.1 R_e$ altitude where they reach their maximum energy.

Figure 10 shows the evolution of ion pitch-angle distributions in altitude. To construct Figure 10, 40 particle trajectories were run simultaneously and the particle's pitch angles were sampled at altitudes 1000 km, 5000 km, 6000 km and 7000 km. These pitch angle "densities" are labeled 1, 5, 6, and 7 in the figure respectively. As expected, the pitch angle distribution at 1000 km altitude is sharply peaked at 90° , with a slight bias toward the upflowing direction. The pitch-angle distribution at 5000 km altitude (within the trapping region in this model) is somewhat bimodal or counter-streaming, again with the upflowing density exceeding the downflowing density due to the escape of some fraction of the particles from the trap. The pitch-angle distributions at 6000 and 7000 km altitude are characteristic of the escaping particles. The distributions are upflowing, and peaked at 128° and 136° , respectively (i.e., conical). Note that the distributions observed above the region of trapping show no evidence of the trap other than enhanced heating — the pitch angle distributions appear exactly as though the ions gained all of their energy at a low altitude mirror point. Again, the simple model presented here is not meant to precisely represent the real world, but rather to demonstrate the effects of trapping on ion energies and trajectories. The altitude distribution of heating and electric fields would certainly affect the resulting ion spectra and pitch angle distributions.

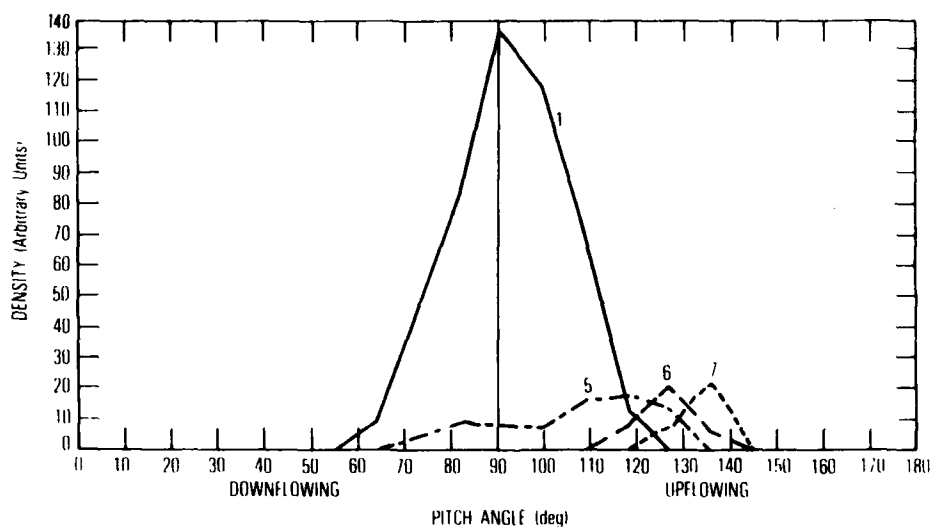


Figure 10. A plot showing the computed ion pitch angle distributions at altitudes 1000, 5000, 6000, and 7000 km.

SUMMARY

Observations of plasmas and electric fields within the regions of space responsible for auroral particle acceleration have verified the existence of electric fields with components parallel to the magnetic field over large altitude regions. Evidence exists that small-amplitude double layers spread along the auroral magnetic field lines provide the mechanism for the maintenance of the auroral potential, although a complete survey of the occurrence of double layers has not yet been accomplished.

Evidence also exists for parallel electric fields directed downward along magnetic field lines in the return current region. Ion conics and upflowing electron beams are also found within the return current regions. These downward parallel electric fields are capable of significantly affecting ion trajectories, and further theoretical investigation of the effects of downward parallel electric fields on ion conic formation is warranted.

REFERENCES

1. P. F. Mizera and J. F. Fennell, Signature of electric fields from high and low altitude particle distributions, *Geophys. Res. Lett.*, 4, 311 (1977).
2. F. S. Mozer, C. W. Carlson, M. K. Hudson, R. B. Torbert, B. Parody, T. Yatteau and M. C. Kelley, Observations of paired electrostatic shocks in the polar magnetosphere, *Phys. Rev. Lett.*, 38, 292 (1977).
3. D. M. Klumpar and W. J. Heikkila, Electrons in the ionospheric source cone: Evidence for runaway electrons as carriers of downward Birkeland currents, *Geophys. Res. Lett.*, 9, 873 (1982).
4. J. L. Burch, P. H. Reiff and M. Sugiura, Upward electron beams measured by DE-1: A primary source of dayside Region-1 Birkeland currents, *Geophys. Res. Lett.*, 10, 753 (1983).
5. D. J. Gorney, D. R. Croley, Jr. and Y. T. Chiu, Trapping of ion conics by downward parallel electric fields, *J. Geophys. Res.*, in press (1984).
6. P. F. Mizera, D. J. Gorney and J. F. Fennell, Experimental verification of an S-shaped shock, *J. Geophys. Res.*, 87, 1535 (1982).
7. M. Temerin, C. Cattell, R. Lysak, M. Hudson, R. Torbert, F. S. Mozer, R. D. Sharp and P. M. Kintner, The small-scale structure of electrostatic shocks, *J. Geophys. Res.*, 86, 11278 (1981).
8. Y. T. Chiu and J. M. Cornwall, On the structures and mapping of auroral electrostatic potentials, *J. Geophys. Res.*, 86, 10029 (1983).
9. M. Ashour-Abdalla and H. Okuda, Plasma physics on auroral field lines: The formation of ion conic distributions, in: *High Latitude Space Plasma Physics*, eds. B. Hultquist and T. Hagfors, Plenum Press, New York 1983, p. 165.
10. P. B. Dusenbery and L. R. Lyons, Generation of ion conic distributions by upgoing ionospheric electrons, *J. Geophys. Res.*, 86, 7627 (1981).
11. L. A. Frank and D. A. Gurnett, Distributions of plasmas and electric fields over the auroral zones and polar caps, *J. Geophys. Res.*, 76, 6829 1971.
12. R. B. Torbert and F. S. Mozer, Electrostatic shocks as the source of discrete auroral arcs, *Geophys. Res. Lett.*, 5, 135 (1978).

13. M. Temerin, K. Cerny, W. Lotko and F. S. Mozer, Observations of double layers and solitary waves in the auroral plasma, *Phys. Rev. Lett.*, in press (1984).
14. F. S. Mozer and M. Temerin, Solitary waves and double layers as electric fields, in: *High Latitude Space Plasma Physics*, eds. B. Hultquist and T. Hagfors, Plenum Press, New York 1983, p. 453.
15. P. M. Kintner, M. C. Kelley, R. D. Sharp, A. G. Ghielmetti, M. Temerin, C. A. Cattell and P. Mizera, Simultaneous observations of energetic upstreaming ions and EHC waves, *J. Geophys. Res.*, 84, 7201 (1979).
16. Y. T. Chiu and M. Schulz, Self-consistent particle and parallel electrostatic field distributions in the magnetospheric-ionospheric auroral region, *J. Geophys. Res.*, 83, 629 (1978).
17. A. G. Ghielmetti, R. G. Johnson, R. D. Sharp and E. G. Shelley, The latitudinal, diurnal and altitudinal distributions of upward flowing energetic ions of ionospheric origin, *Geophys. Res. Lett.*, 5, 59 (1978).
18. D. J. Gorney, A. Clarke, D. Croley, Jr., J. Fennell, J. Luhmann and P. Mizera, The distribution of ion beams and conics below 8000 km, *J. Geophys. Res.*, 86, 83 (1981).
19. D. A. Bryant, Hot electrons in and above the auroral ionosphere: Observations and physical implications, in: *High Latitude Space Plasma Physics*, eds. B. Hultquist and T. Hagfors, Plenum Press, New York 1983, p. 295.
20. C. A. Cattell, The relationship of field-aligned currents to electrostatic ion cyclotron waves, *J. Geophys. Res.*, 86, 3641 (1981).
21. P. M. Kintner and D. J. Gorney, A search for the plasma processes associated with perpendicular ion heating, *J. Geophys. Res.*, 89, 937 (1984).
22. T. Chang and B. Coppi, Ion acceleration by lower hybrid modes, *Geophys. Res. Lett.*, 12, 12153 (1981).

LABORATORY OPERATIONS

The Laboratory Operations of The Aerospace Corporation is conducting experimental and theoretical investigations necessary for the evaluation and application of scientific advances to new military space systems. Versatility and flexibility have been developed to a high degree by the laboratory personnel in dealing with the many problems encountered in the nation's rapidly developing space systems. Expertise in the latest scientific developments is vital to the accomplishment of tasks related to these problems. The laboratories that contribute to this research are:

Aerophysics Laboratory: Launch vehicle and reentry fluid mechanics, heat transfer and flight dynamics; chemical and electric propulsion, propellant chemistry, environmental hazards, trace detection; spacecraft structural mechanics, contamination, thermal and structural control; high temperature thermomechanics, gas kinetics and radiation; cw and pulsed laser development including chemical kinetics, spectroscopy, optical resonators, beam control, atmospheric propagation, laser effects and countermeasures.

Chemistry and Physics Laboratory: Atmospheric chemical reactions, atmospheric optics, light scattering, state-specific chemical reactions and radiation transport in rocket plumes, applied laser spectroscopy, laser chemistry, laser optoelectronics, solar cell physics, battery electrochemistry, space vacuum and radiation effects on materials, lubrication and surface phenomena, thermionic emission, photosensitive materials and detectors, atomic frequency standards, and environmental chemistry.

Computer Science Laboratory: Program verification, program translation, performance-sensitive system design, distributed architectures for spaceborne computers, fault-tolerant computer systems, artificial intelligence and microelectronics applications.

Electronics Research Laboratory: Microelectronics, GaAs low noise and power devices, semiconductor lasers, electromagnetic and optical propagation phenomena, quantum electronics, laser communications, lidar, and electro-optics; communication sciences, applied electronics, semiconductor crystal and device physics, radiometric imaging; millimeter wave, microwave technology, and RF systems research.

Materials Sciences Laboratory: Development of new materials: metal matrix composites, polymers, and new forms of carbon; nondestructive evaluation, component failure analysis and reliability; fracture mechanics and stress corrosion; analysis and evaluation of materials at cryogenic and elevated temperatures as well as in space and enemy-induced environments.

Space Sciences Laboratory: Magnetospheric, auroral and cosmic ray physics, wave-particle interactions, magnetospheric plasma waves; atmospheric and ionospheric physics, density and composition of the upper atmosphere, remote sensing using atmospheric radiation; solar physics, infrared astronomy, infrared signature analysis; effects of solar activity, magnetic storms and nuclear explosions on the earth's atmosphere, ionosphere and magnetosphere; effects of electromagnetic and particulate radiations on space systems; space instrumentation.

...

ATE
LMED
-8